metals

MDPI

Article

Finite Modeling and Simulation of the Effects of Neutral Electrolytic Pickling Process Parameters on EN 1.4404 Steel Strips

Arif Tirto Aji [1], Jari Aromaa [1,*], Teemu Tuovinen [2,3], Elina Riekki [2] and Mari Lundström [1]

[1] School of Chemical Engineering, Aalto University, P.O. Box 16200, FI-00076 Espoo, Finland; aaji2@fmi.com (A.T.A.); mari.lundstrom@aalto.fi (M.L.)
[2] Research Center, Outokumpu Stainless Oy, FI-95490 Tornio, Finland; teemu.tuovinen@oulu.fi (T.T.); elina.riekki@outokumpu.com (E.R.)
[3] Research Unit of Sustainable Chemistry, University of Oulu, P.O. Box 3000, FI-90014 Oulu, Finland
* Correspondence: jari.aromaa@aalto.fi

Abstract: Surface treatment via neutral electrolytic pickling (NEP) aims to remove oxide layers and scaling from stainless steel. The objective of this study was to investigate the factors that affect the energy efficiency of the process. This study developed a COMSOL Multiphysics model for the distribution of current across a bipolar steel strip by controlling the following parameters: Na_2SO_4 concentration, temperature, electrode-to-strip distance, and inter-electrode distance. Full factorial measurements of the electrolyte's conductivity as well as the steel strip's and the electrode's polarization were conducted to provide data for the NEP model. Galvanostatic pulse measurements were performed to calculate transient times during pickling. According to the model, an applied voltage of less than 11 V was insufficient to polarize the steel strip to the potentials needed on both the anodic and cathodic sides. A higher voltage of 11–15 V resulted in anodic current densities of 600–1600 A m^{-2} and cathodic current densities of 700–2000 A m^{-2} on the steel strip. These current densities are within the range of previous experimental studies and industrial practices. The model showed that when a steel strip acts as a bipolar electrode, the current's efficiency decreases, as only a fraction of the strip facing the anodes or cathodes is polarized sufficiently. The galvanostatic tests showed that anodic polarization of the steel strip is easier than cathodic polarization. The slow polarization in the cathodic direction can be improved by using a higher current density. The time needed to polarize stainless steel indicates that the strip's velocity should be less than 1 m s^{-1} to give enough time for polarizing the steel strip.

Keywords: neutral electrolytic pickling; stainless steel; finite modeling

Citation: Aji, A.T.; Aromaa, J.; Tuovinen, T.; Riekki, E.; Lundström, M. Finite Modeling and Simulation of the Effects of Neutral Electrolytic Pickling Process Parameters on EN 1.4404 Steel Strips. *Metals* **2023**, *13*, 2001. https://doi.org/10.3390/met13122001

Academic Editor: Rastko Vasilic

Received: 1 September 2023
Revised: 14 November 2023
Accepted: 22 November 2023
Published: 12 December 2023

1. Introduction

The production of stainless steel includes rolling and reheating, which produce oxide layers on the steel's surface [1]. The formation of an oxide layer is affected by the steel's composition; in particular, manganese and chromium have a high affinity toward oxygen. Forming steel, either via hot or cold rolling, affects the formation of oxide layers. Chromium oxide formation was found to happen with the cold rolling of steels [2,3], while hot rolling forms more iron-rich oxides [4,5]. Characterization studies have shown numerous compositions of the oxide layer, as shown in Table 1. To remove the oxide layer, pickling is performed in several stages, from mechanical descaling and preliminary pickling to final pickling [1]. Removal of the oxide scale is important to ensure the passivation and corrosion resistance of stainless steel [6].

Table 1. Characterization of the oxide layers on steels.

Alloy Type	Oxide Scale	References
EN 1.4301, Cr (5.76–26.31%) steels	Cr_2O_3, α-Fe_2O_3, $(Fe,Cr)_3O_4$	[7–12]
EN 1.4016, EN 1.4762, microalloyed steel, Incoloy 800 (Cr 19–23%, Ni 30–35%)	FeO, Fe_2O_3, Fe_3O_4	[4,8,10,12–16]
EN 1.4301, EN 1.4016	$NiFe_2O_4$, Fe_3O_4, $(Fe,Cr)_2O_3$ (with Fe^{2+}, Fe^{3+} and Cr^{3+})	[2,17]
EN 1.4301, EN 1. 4016	$(Fe, Cr)_2O_3$ (with Fe^{2+}, Fe^{3+} and Cr^{3+})	[18]
	Cr_2O_3	[6,19,20]
Carbon steel, interstitial-free steel	FeO, Fe_2O_3, Fe_3O_4, FeO(OH)	[21,22]

Chemical or electrochemical pickling processes have been intensively developed with an aim toward being efficient and environmentally friendly processes. Straight sulfuric acid is not always effective, and the use of combinations of hydrochloric and nitric acids could result in pitting. Such pickling solutions are expensive and release poisonous gases and fumes. Nead's patent in 1924 pointed out that cold rolling would mechanically break the oxide film, assisting in acid pickling after hot rolling [23]. In 1931, Elder proposed the use of copper with sulfuric acid [24], and Schermer proposed the addition of alkali metal nitrates to sulfuric acid [25]. Hahn patented the use of a mixture of sulfuric and nitric acids in 1956 [26]. Due to concerns regarding the environmental and occupational impact of various acidic pickling processes, electrolytic pickling using a neutral electrolyte was introduced by Ruthner Industrieanlagen AG in Austria at the end of the 1950s [27]. Neutral electrolytic pickling uses neutral or near-neutral Na_2SO_4 to reduce acid effluents and improve the products' quality [27]. Electrolytic pickling operates at elevated temperatures up to 90 °C and at high current densities up to 3000 A/m^2 [28–31]. These values indicate that electrolytic pickling is an energy-intensive process. Furthermore, of the current supplied to a pickling cell, only 20–30% is used in the polarization of stainless steel. If we consider the side reactions on the steel's surface, the current efficiency of oxide scale removal can be less than 10% [32].

A schematic of a pickling cell is shown in Figure 1. The cell is divided into three regions, marked E1, E2, and E3. The steel strip moves between electrode pairs. The steel strip is not connected to an external current source, nor is it grounded, so it acts as a bipolar electrode. The electrode pairs in regions E1 and E3 are polarized as cathodes, and the steel strip opposite to them acts as an anode. The electrodes in the middle region (E2) are polarized as anodes, and the steel strip opposite to them acts as a cathode. The steel strip becomes a bipolar electrode when the potential field strength between the polarized anodes and cathodes is strong enough. Factors that will affect the potential field strength are the operating current density and the system's geometry. The system's geometry includes the length of the electrodes, the distance between the electrodes, and the electrode-to-strip distance. The steel strip is polarized just opposite the current-feeding electrodes. In the setup shown in Figure 1 with identical electrode sizes, the cathodic strip current density opposite E2 is twice the anodic current density opposite E1 and E3.

An industrial neutral electrolytic pickling line is tens of meters long. The line has several electrode banks, as shown in Figure 1. The banks are slightly inclined to promote the transfer of gas bubbles away from the electrodes and strip. The anodes are often strips of lead, while the cathodes are made of unalloyed steel, again to promote the removal of bubbles. The length of one anode or cathode pack is typically 1–1.5 m, and the distance between anode and cathode packs is 0.5–1 m. The distance from the electrode packs to the stainless steel strip is 10–15 cm. One electrode bank is supplied by a DC rectifier, which can typically have an output capacity of 10 kA or more. During operation, the output voltage

of a rectifier can be over 40 V, depending on the operating current density. The strip moves through the pickling bath with a speed of the order of 1 m s^{-1}. The time that a section of a moving steel strip spends between the electrodes is short, and the polarization phenomena on the strip can be interpreted as short galvanostatic pulses, which can last less than 1 s.

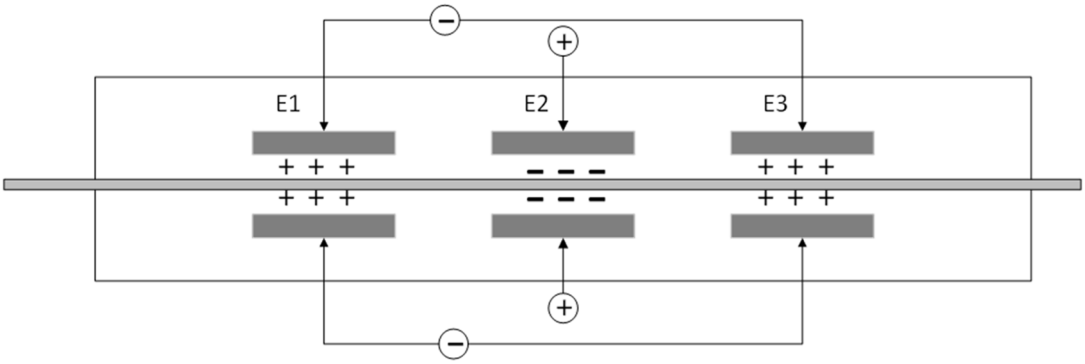

Figure 1. Schematic diagram of an electrolytic bipolar pickling cell, adapted from [33].

Several mechanisms of steel pickling have been proposed, such as dissolution of the oxide scale [27]; partial dissolution of the oxide scale; dissolution of the metallic species; gas evolution, which mechanically cracks the oxide scale [31,34]; electrochemical dissolution of chromium and manganese [9,19,35]; and dissolution of the subscale metal under the oxide scale [9,36,37]. During the pickling process, the electrochemical reaction on the lead anode is oxygen evolution (1), and that on the steel cathode is hydrogen evolution (2) via the decomposition of water. Depending on the stainless steel strip's polarization, the oxygen evolution can happen as a side reaction that does not assist in dissolving the oxide film.

$$2\,H_2O \rightarrow 4\,H^+ + O_2(g) + 4\,e^- \quad (1)$$

$$4\,H_2O + 4\,e^- \rightarrow 4\,OH^- + 2\,H_2(g) \quad (2)$$

As seen from the reactions in Equations (1) and (2), to maintain the electric charge and pH balance, the amount of hydrogen gas produced on the cathodes is two times that of the oxygen produced on the anodes. With the bipolar circuit shown schematically in Figure 1 and assuming electrodes of an identical size, the current density on the steel cathodes will be half that on the lead anodes. Furthermore, if we assume that only the areas of the stainless steel strip opposite the anodes and cathodes will polarize, then the anodic current density on the strip is half that of the cathodic current density. This means that the surface of the strip in the anodic sections E1 and E3 will polarize less than in the cathodic section E2, as shown in Figure 1.

On the anodic parts of the strip's surface, the possible reactions include oxidation of the oxide film's compounds to a higher valence state, resulting in their dissolution, the dissolution of the metals in the stainless steel, and oxygen evolution. The chromium in $(Fe,Cr)_2O_3$ or $FeCr_2O_4$ is in a trivalent state, and it can oxidize to Cr^{6+} or $Cr_2O_7^{2-}$. The iron in $FeCr_2O_4$ is in a divalent state, and it can oxidize to Fe^{3+} or ferrate FeO_4^{2-}, the latter of which is unstable in acidic or neutral solutions. Manganese can oxidize to MnO_4^- [1]. In the neutral electrolyte, the cations released from the dissolution of either oxide or metal can hydrolyze and form hydroxides [27]. The manganese- and chromium-enriched films dissolve first during anodic polarization, followed by dissolution of the iron-rich layer. The chromium-depleted layer and the silicon-containing layers do not dissolve during anodic polarization [1,6,19]. On the cathodic parts of the strip, the main reaction is the hydrogen evolution, as shown in Equation (2). The hydrogen evolution can assist in the removal of the oxide film through the mechanical action of gas bubbles.

Increasing the efficiency of the electrolytic pickling process has been a challenge. The factors affecting the pickling process can be grouped into internal factors related to the stainless steel strips and external properties that are not dependent on the steel. The internal

properties include steel's polarization behavior, both as an anode and a cathode, and the steel strip's electrical resistance. The external factors expected to affect the efficiency of the process are the physicochemical properties of the electrolyte (i.e., its conductivity, density, and viscosity), the cell's geometry, the externally applied potential, and the steel strip's velocity. This study aimed to develop a COMSOL Multiphysics model to investigate the effect of the processing parameters on the distribution of the current and potential. Similar studies were not found in the available literature. Electrochemical tests were used to determine the polarization of the stainless steel strips and the lead and steel electrodes. The properties of the electrolyte were determined. These results were used as factors to build the model. Based on the literature, our hypotheses were that the potential field between the anodes and cathodes would result in an uneven polarization of the stainless steel strip, the strip's polarization would depend only on the applied current, and the electrolyte's conductivity would affect the potential field.

2. Materials and Methods

Measurements were conducted in electrolytes with 150–200 g dm^{-3} of Na_2SO_4 at 60–80 °C. The experiments included modeling the conductivity, modeling the polarization, and transient measurements. The parts of this study and their links are shown in Figure 2.

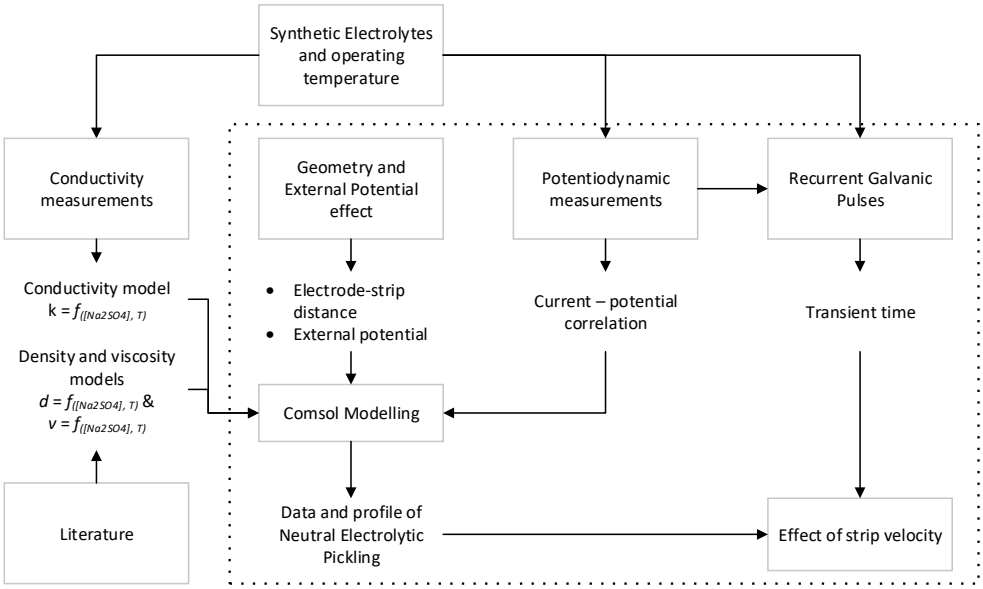

Figure 2. Schematic of the method used in this study.

Conductivity was measured using a Knick Portamess® 913 conductivity meter (Elektronische Messgeräte GmbH & Co. KG, Berlin, Germany), and the calibration was conducted using a solution with a standard conductivity of 12.88 mS cm^{-1} at 25 °C (Reagecon, Clare, Republic of Ireland). The electrochemical measurements were conducted in two parts. Firstly, the behavior of the steel strip and the electrodes in different electrolytes was measured using the potentiodynamic method with a Gill-AC potentiostat from ACM instruments with a calomel reference electrode, +0.2415 V vs. SHE, and a platinum counter-electrode. Measurements of each anodic and cathodic region of the steel were conducted separately, up to an overpotential of 3 V in the respective direction.

Tafel plots (Equations (3) and (4)) of the active region of the electrodes and strip were used to describe the current density–potential dependence. Figure 3 shows how the procedure was applied to the lead anode and steel cathode. The starting point, E_{start} and i_{start}, was determined as the intersection of the active range and the range where no significant reactions had happened. The slope of the active range b was calculated as the V per decade of current density. These equations were used in the COMSOL model to represent the electrodes and the steel strip. At the highest current densities, all materials

showed a clear deviation from the Tafelian behavior due to the uncompensated resistance of the solution. This range was not included in the analysis used to determine the factors for Equations (3) and (4).

$$E = E_{start} + log\left(\frac{i}{i_{start}}\right) \cdot b \tag{3}$$

$$i = i_{start} \cdot 10^{\left(\frac{(E-E_{start})}{b}\right)} \tag{4}$$

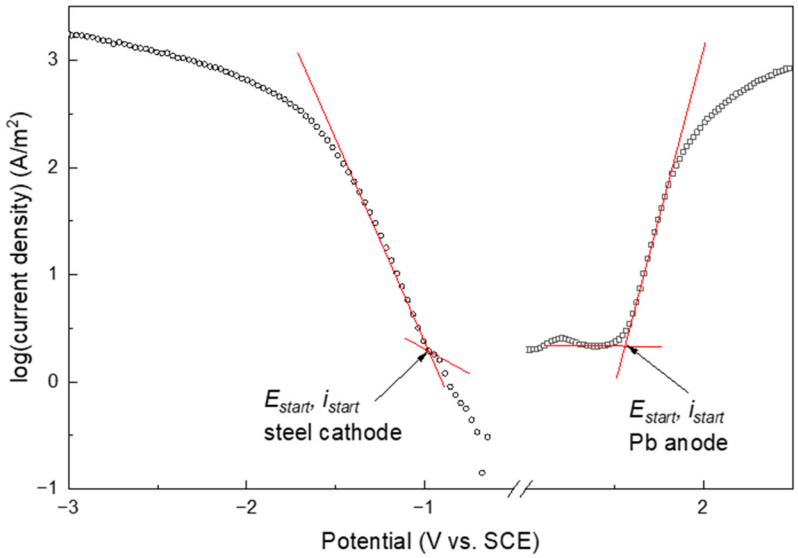

Figure 3. Determination of the starting point for calculating the active range of the steel cathode and the lead anode.

The second study involved transient measurements of the galvanostatic pulse using a Versastat 4 potentiostat from Princeton Applied Science, with a range of current densities from 200 A m^{-2} to 1800 A m^{-2}, a 10 s pulse time, and five cycles for each measurement (Figure 4). This range of current density was within the industrial range of current density, and the results from the potentiodynamic measurements are shown schematically in Figure 3. The objective of this measurement was to determine the time needed for the steel strip to reach a steady potential once it had been introduced into a certain potential field.

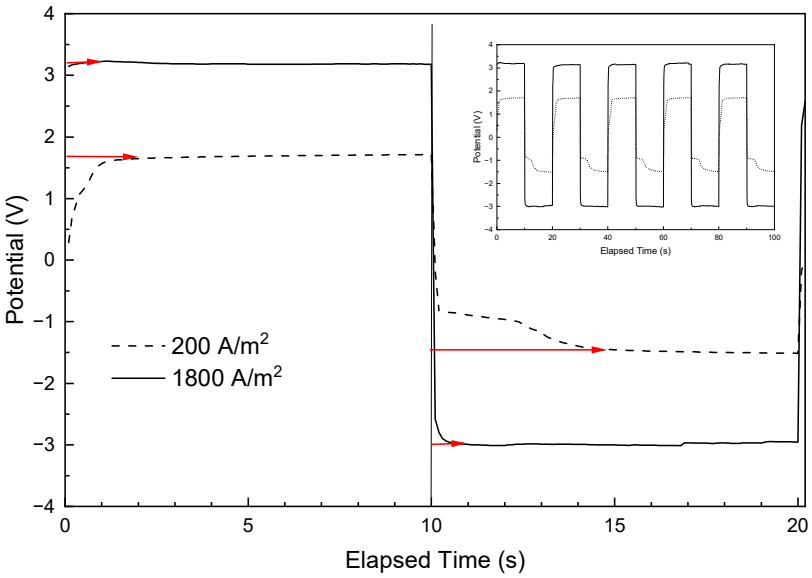

Figure 4. Estimation of the time to steady-state polarization.

Modeling was conducted with COMSOL Multiphysics 5.6 software. The model was a half-cell of the standard industrial setup (Figure 1) due to the symmetry of the top and bottom halves of the system, and the geometry is presented in Figure 5. The anodes and cathodes were located only under the strip. The parameters of the COMSOL model are shown in Table 2, and the material properties of the solid electrodes were provided by the built-in data of the COMSOL 5.6 software. The range of distance from the electrode to the steel strip was 10–15 cm, according to industrial experience of the authors.

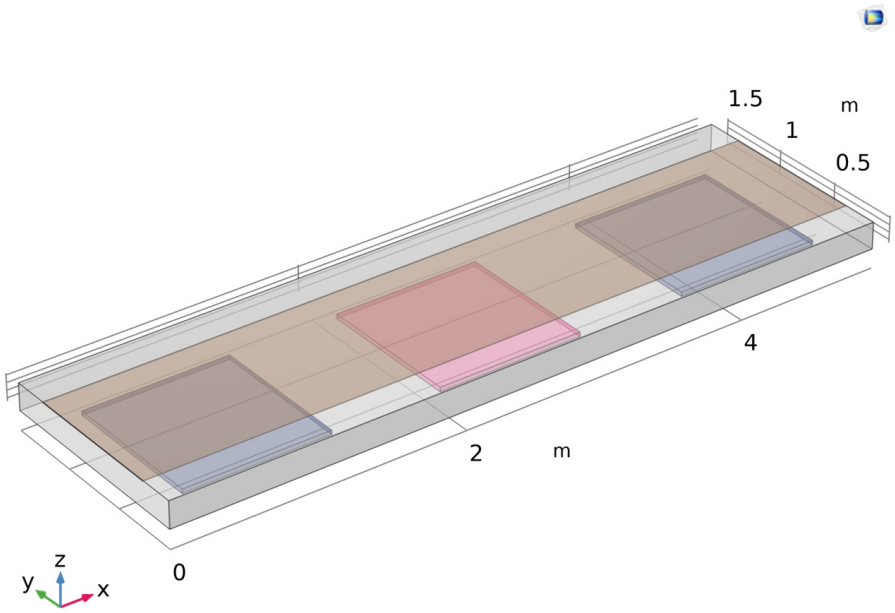

Figure 5. Half-cell geometry of the COMSOL model, showing the configuration of the steel and electrodes, where the brown rectangle is the steel strip and the blue and red rectangles are the cathodes and anode, respectively. The model's dimensions are in meters.

Table 2. Modeling constants and variables of the electrochemical measurements. Test values marked with * are the center points of the factorial test series.

Model Parameter	Value	Model Variables	Values
Anode–cathode distance	50 cm	Concentration of Na_2SO_4	150, 175 *, 200 g dm^{-3}
Length of anode and cathode	1 m	Temperature	60, 70 *, 80 °C
Width of electrodes and steel	1 m	Steel–electrode distance	10, 12.5, 15 cm
Thickness of the strip	3 mm		

3. Results and Discussion

3.1. Physicochemical Properties of the Electrolyte

The electrolyte, as the medium of the process, has significant importance for the development of a representative model, as it affects the operating voltage of the system. Thus, the electrolyte's density, viscosity, and conductivity were modeled. The determination of the multilinear regression equations was achieved with the Microsoft Excel Regression tool using a confidence level of 95%. The modeling of the density, viscosity, and conductivity used data from [38] for 0.05–1.5 mol kg^{-1} of Na_2SO_4 at 15–55 °C; in addition, a series of conductivity measurements were carried out at higher temperatures. The regression models for density, viscosity, and conductivity are shown in Equations (5)–(7). The concentration of Na_2SO_4 is given in g dm^{-3}, and the temperature is in °C.

$$\rho\ [\text{kg m}^{-3}] = 1007.3 + 0.815\ c - 0.321\ T - 0.001\ c\ T \quad (5)$$

$$\eta\ [\text{mPa·s}] = 1.286 + 0.005\ c - 0.015\ T - 4.4\ 10^{-5}\ c\ T \quad (6)$$

$$\kappa\ [\text{S m}^{-1}] = 8.11 - 0.024\ c + 0.019\ T + 0.001\ c\ T \quad (7)$$

Figure 6 shows the values of these properties within the modeling ranges shown in Table 2. The density was 1090–1140 kg m^{-3}, the viscosity was 0.20–0.74 mPa·s, and the conductivity was 17.3–25.6 S m^{-1}.

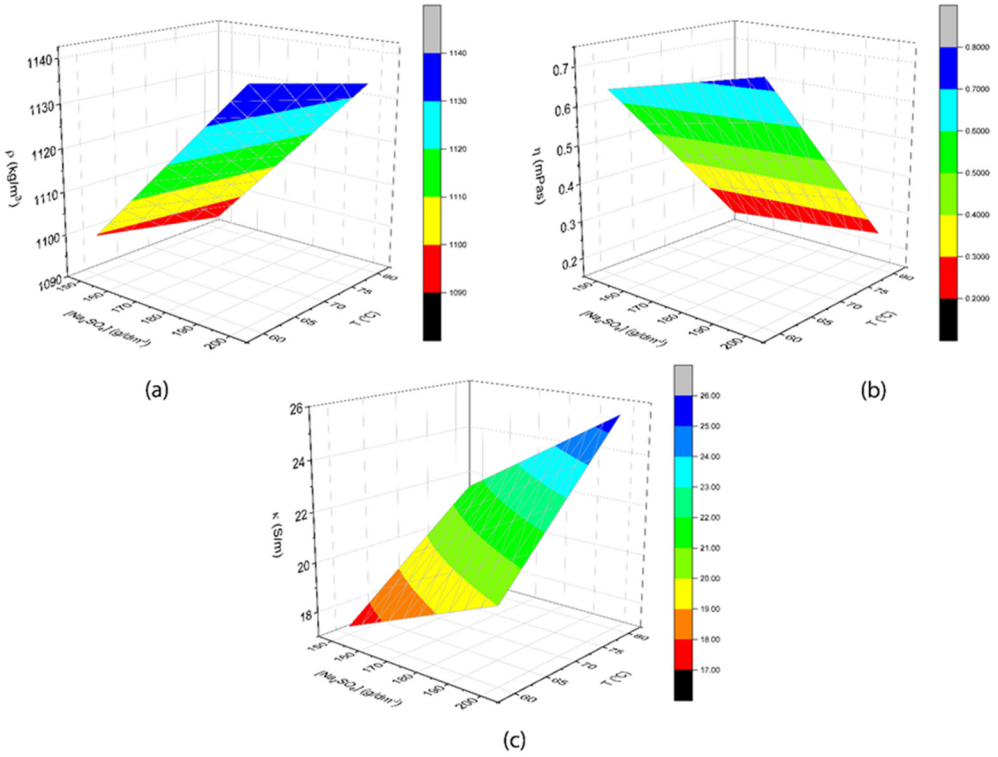

Figure 6. Physicochemical properties of NEP: density (**a**), viscosity (**b**), and conductivity (**c**).

3.2. Polarization of the Electrodes and the Steel Strip

The objective of the polarization measurements was to provide empirical models for the potential–current density dependence of the active surfaces of the lead anode, the steel cathode, and the stainless steel strip. These models were used in the Comsol software package to calculate the current density across each surface. From a total of 12 measurements for each material (the lead anode, the carbon steel cathode, the stainless steel anode, and the stainless steel cathode), selected polarization curves are presented in Figure 7.

Figure 7 shows that, when the steel cathode and the stainless steel cathode were polarized, the current started to increase almost immediately. This was due to the main reaction in these materials being hydrogen evolution. The lead anode needed significant polarization to about 1.8 V before the rate of oxygen evolution was in the 100 A m^{-2} range (Figure 7). Trans-passive dissolution, with or without the oxygen evolution on the stainless steel, also needed significant polarization with a dissolution rate in the range of 100 A m^{-2} at about 1.6 V. All four sets of polarization curves showed a clear deviation from a linear E vs. log(i) behavior at high current densities. This was due to a drop in the ohmic voltage in the electrolyte, the magnitude of which depended on the test system's geometry and the electrolyte's conductivity.

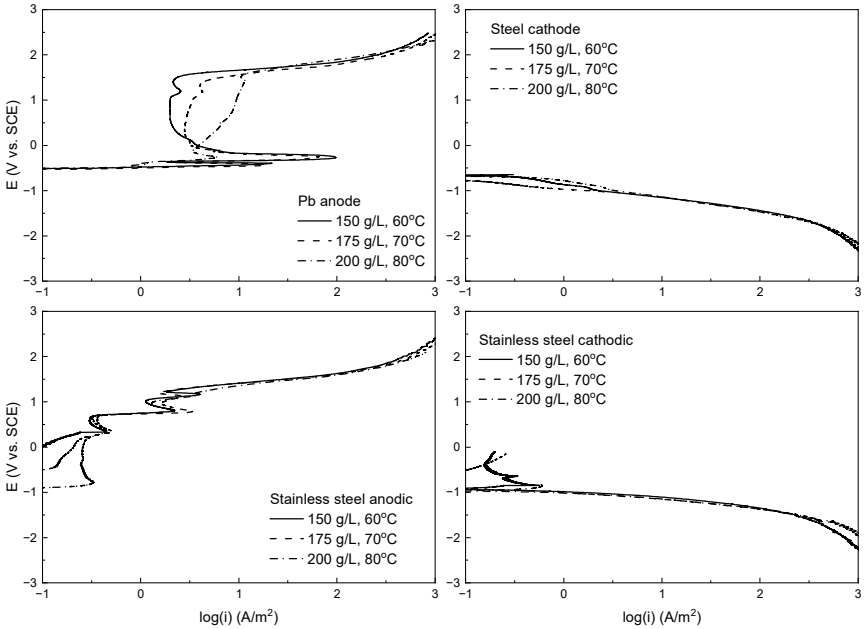

Figure 7. Selected polarization measurements of the lead anode, the steel cathode, and EN 1.4404 stainless steel as the anode and cathode.

The effect of the electrolyte's conditions was insignificant, as can be seen from a comparison of the least conductive (150 g dm^{-3} Na_2SO_4 at 60 °C), central (175 g dm^{-3} at 70 °C), and most conductive (200 g dm^{-3} at 80 °C) electrolytes in Figure 7. The polarization curves overlapped each other in the active range, where the *E*–log(*i*) dependence was linear. Unlike the electrolyte's properties, the concentration of Na_2SO_4 and temperature had no statistically significant effect on the starting potentials, current densities, or Tafel slopes. Therefore, the starting potentials, current densities, and Tafel slopes were taken as the average values for Equations (3) and (4). Through the use of these average values, kinetic formulas (Equations (8)–(11)) were developed to calculate the current density, where *E* refers to the electrode's potential, V, vs. SCE.

$$Lead\ anode: i\left[\mathrm{A\ m^{-2}}\right] = 3.3{\cdot}10^{(E-1.39)/0.24} \quad (8)$$

$$Steel\ cathode: i\left[\mathrm{A\ m^{-2}}\right] = 0.3{\cdot}10^{(E+0.68)/-0.29} \quad (9)$$

$$Stainless\ as\ anode: i\left[\mathrm{A\ m^{-2}}\right] = 2.2{\cdot}10^{(E-1.14)/0.27} \quad (10)$$

$$Stainless\ as\ cathode: i\left[\mathrm{A\ m^{-2}}\right] = 3.3{\cdot}10^{(E+1.07)/-0.26} \quad (11)$$

3.3. Multiphysics Modeling

Modeling was conducted for a half-cell model of the industrial NEP process (Figure 5). The electrolyte's properties were taken as functions of the concentration of Na_2SO_4 and the operating temperature, as shown in Equations (5)–(7), and the electrode's polarization was calculated using Equations (8)–(11). The material properties of the lead, steel grade 4310, and stainless steel grade 316L were taken from the internal database of the COMSOL material library. The secondary current distribution module was selected for this study. The current was enclosed inside the geometry of the system by insulating the cells' boundaries. The external potential of the steel strip was set to 0, so the steel would be polarized indirectly by the anode's and cathode's potential fields. Finally, the total voltage was equally assigned to the external potential applied by the anode and cathode. Different potential fields formed when an external potential was applied to the cell through the surfaces of the lead anode

and the steel cathode (Figure 8). Different intensities of these fields were computed using different conditions of the electrolyte.

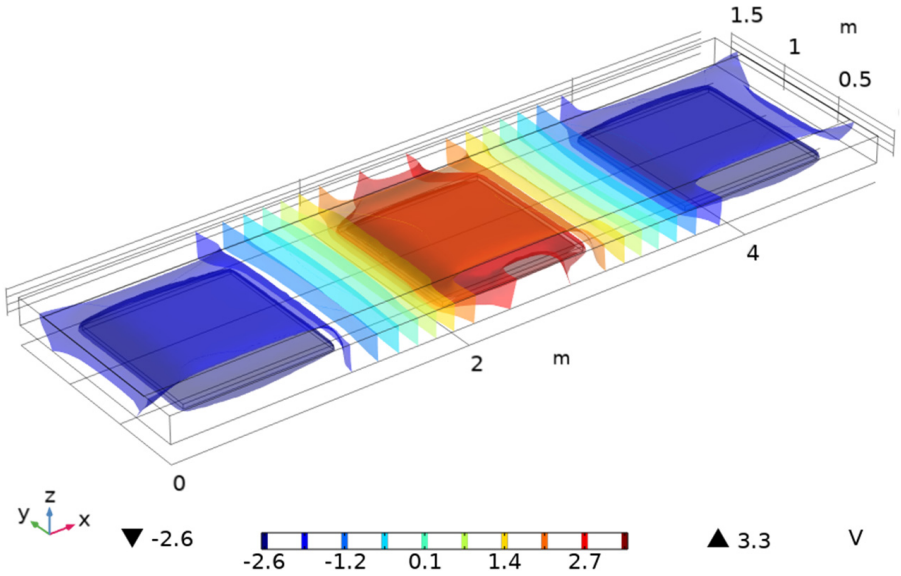

Figure 8. Potential fields in the electrolyte, showing the effects of the two cathodes (both edges) and the anode (center) when an external voltage of 15 V was applied.

A stationary study with a cell voltage of 5 to 15 V was conducted for each set of values for the concentration, temperature, and steel–electrode distance (Table 2). The values of the potential and current density were modeled across the length of the steel strip. Selected results of the COMSOL modeling are shown in Figures 9 and 10 for the potential and current density profiles, respectively. The different conditions of the electrolyte with the lowest and highest conductivity were compared.

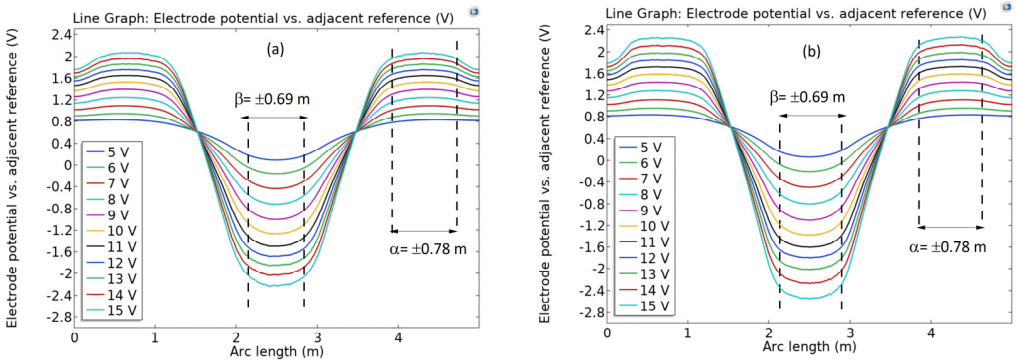

Figure 9. Selected potential profile across the steel strip for an external potential range of 5–15 V for (**a**) 150 g dm^{-3} of Na_2SO_4, 60 °C and 15 cm distance and (**b**) 200 g dm^{-3} of Na_2SO_4, 80 °C and 10 cm distance.

Figure 9 shows the bipolar behavior of the steel strip along the length of the *x*-axis. As can be seen, the polarizations were opposite to the electrolyte's potential field in Figure 8. The steel strip was anodically polarized on both edges, while, at the center, it was cathodic. The steel strip's polarization increased with an increase in the applied external voltage. When the applied external voltage was 5–15 V, it was calculated that only 40–50% of the steel strip's surface was sufficiently polarized. This value is within the range of previous studies, which indicated 40% from direct measurements of the current [32] and 60–65% calculated by mathematical modeling [39]. The loss of potential was mainly due to the electrolyte's resistance.

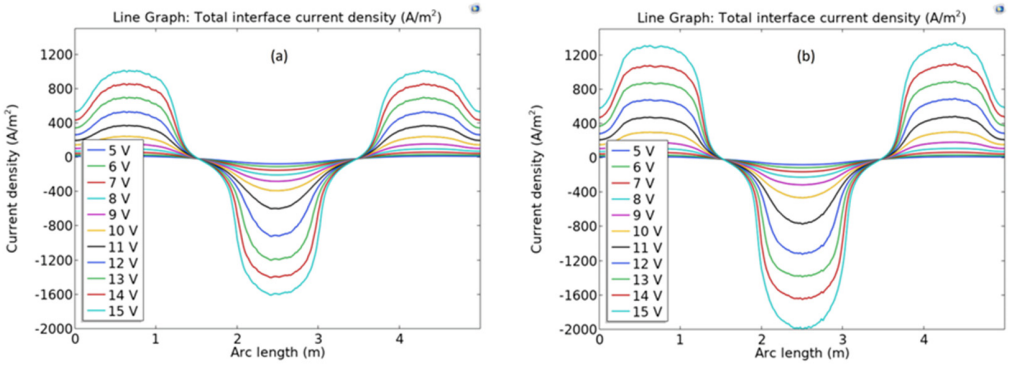

Figure 10. Current density profile across the steel strip for an external potential range of 5–15 V for (**a**) 150 g dm^{-3} of Na_2SO_4, 60 °C and 15 cm distance and (**b**) 200 g dm^{-3} of Na_2SO_4, 80 °C and 10 cm distance.

Figure 10 shows that the current density also increased, along with an increase in the external voltage. Nevertheless, the increase in the current density was not linear with the voltage, unlike the strip potential. The current density increased clearly beyond 11 V of external voltage. This was consistent with the Tafelian behavior shown in Equations (10) and (11). The external voltage between the lead anode and steel cathodes resulted in a potential field that, in turn, polarized the strip's surface. As the current density of the strip's surface increased exponentially with increasing polarization, significant current densities on the strip were seen only when the external voltage was sufficiently high. Figure 10 shows that, even though the electrolyte's properties did not affect the polarization behavior of the electrodes (as shown in Figure 7), a significant part of the polarizing power was lost to the electrolyte's resistance. Nevertheless, the calculated current densities were within the industrial levels of 500–3500 A m^{-2} reported in numerous studies [31,32,40].

Another result from the potential profile in Figure 9 was the effective polarized area. When the length of the lead anodes and the steel cathodes was set to 1 m and their horizontal distance was set to 0.5 m, the strip's surface had a shorter area under the electrodes where the potential was steady. The surface of the anodically polarized steel had a more polarized surface area (α = 0.78 m) compared with the cathodic equivalent (β = 0.69 m). Thus, in the total length of an NEP electrode bank, the steel is under anodic polarization for 2.3 times longer than it is under cathodic polarization. The narrow range of the full cathodic potential is beneficial for the process, as excessive exposure to hydrogen, which can embrittle the steel's surface, is limited.

3.4. Effect of the Electrolyte, External Potential, and Geometry

The conditions of the electrolyte, the external potential, and the cell's geometry are parameters that potentially affect the profile of the current density on the strip's surface. To estimate the magnitude of each effect, the anodic and cathodic currents were calculated using the COMSOL model, and the peak values shown in Figure 10 were selected. The variables were the same as in Table 2 with the addition of 11–15 V of external voltage. A statistical analysis of the anodic and cathodic currents was carried out using the Microsoft Excel Regression tool. The regression equations for the peak anodic and cathodic currents on the steel strip are shown in Equations (12) and (13), where c is the concentration of Na_2SO_4 in g dm^{-3}, T is the temperature in °C, d is the electrode-to-strip distance in cm, and E_{ext} is external voltage of the cell in V. Note that Equation (13) gives the absolute value of the cathodic current.

$$i_a\left[\text{A m}^{-2}\right] = -1505 + 1.08{\cdot}c + 0.65{\cdot}T - 24.16{\cdot}d + 180.7{\cdot}E_{ext} \quad (12)$$

$$|i_c|\left[\text{A m}^{-2}\right] = -1990 + 0.96{\cdot}c + 0.58{\cdot}T - 35.90{\cdot}d + 268.2{\cdot}E_{ext} \quad (13)$$

Equations (12) and (13) show that both the concentration of Na_2SO_4 and the temperature have positive effects on the stainless steel strip's polarization. Within the test parameter range used in modeling, their combined effect from the lowest to highest values of the parameters was only about 70 A m^{-2} for both the anodic (Equation (12)) and cathodic (Equation (13)) current. The electrode-to-steel strip distance had a clear negative effect on the current density. If we compare the largest and smallest distance, the effect was about -120 A m^{-2} for the anodic polarization and -180 A m^{-2} for the cathodic polarization of the strip. The strongest single-factor effect was the external voltage. Within the calculated voltages (11 V to 15 V), the increase in current density was about 720 A m^{-2} for the anodic polarization and 1070 A m^{-2} for the cathodic polarization of the strip. Figure 11 shows the anodic and cathodic current densities calculated using Equations (12) and (13) when the electrolyte's properties were set to their central values (c = 175 g dm^{-3} and T = 70 °C). The cathodic current density was higher because the current passing through the cell, as well as one electrode bank, went from a single anode to two cathodes. Therefore, the cathodic part of the strip facing the anode polarized more strongly, resulting in higher current densities.

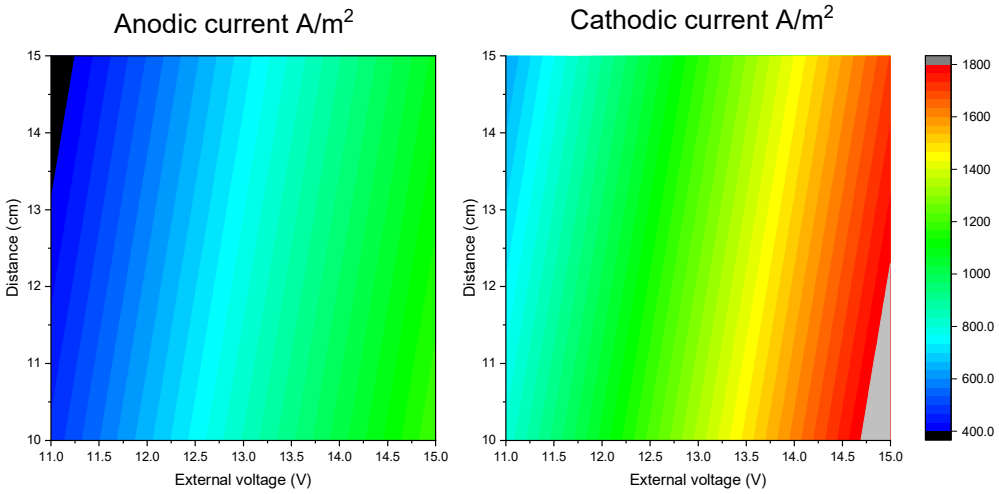

Figure 11. The effects of the external voltage and electrode-to-strip distance on the anodic and cathodic current density; c = 175 g dm^{-3} and T = 70 °C.

3.5. Transient Time

The electrode bank is polarized using a constant current, creating a potential field. When the stainless steel strip enters this field, its surface is polarized, and the reactions result in the cleaning of the surface. The strip travels in the pickling bath at speeds of up to 1 m s^{-1}, and the time the strip faces an electrode can be less than 1 s. When a current step is imposed upon an electrode, the current contains double-layered charging and electrochemical reactions. The double-layered charging current decreases rapidly with time and the Faradaic current due to an increase in the electrochemical reactions. If the time is too short, then the electrochemical reactions do not have time to work on the strip's surface.

The transient time was studied using alternating positive and negative galvanostatic pulses applied to the steel samples. The absolute current density was measured from 200 A m^{-2} to 1800 A m^{-2}. Examples of the galvanostatic tests are shown in Figure 12, where the potential was calculated as the overpotential from the open circuit's potential. The general result from these measurements was that a higher current density resulted in a shorter transient time. Steady anodic potentials were observed at a lower applied current density than the cathodic potentials, and cathodic polarization at low current densities was a two-step process.

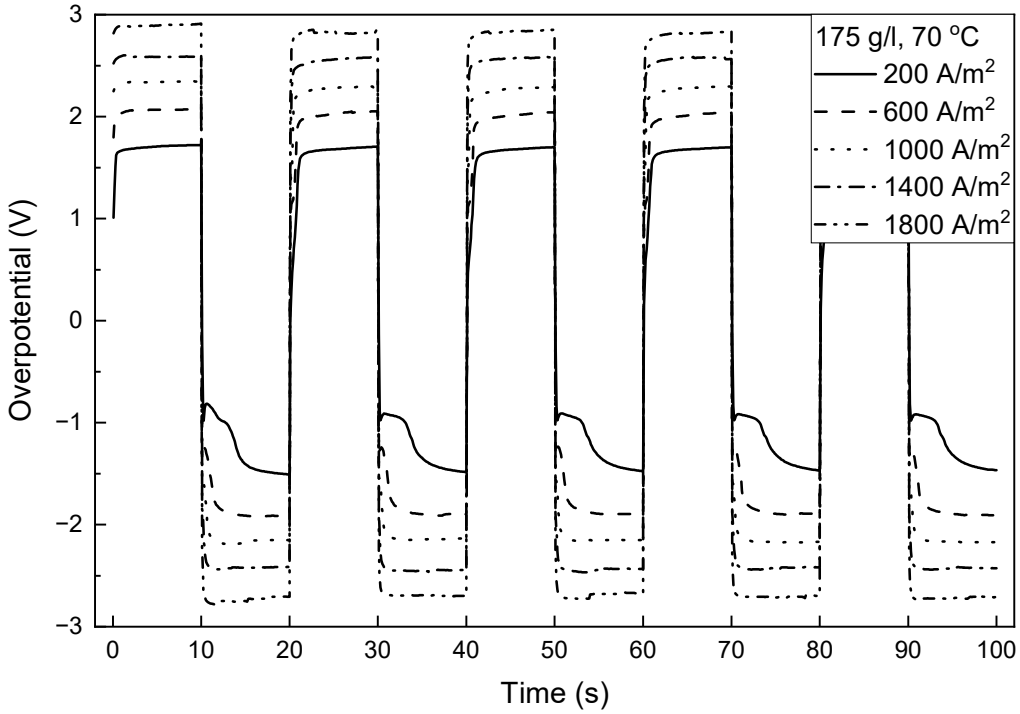

Figure 12. Examples of the galvanostatic transient time measured in 175 g dm^{-3} of Na_2SO_4 at 70 °C.

The transient measurements were analyzed by selecting the first time points after each change in polarization, where dE/dt was 0.01 V/s or less. With the lowest current densities, the time was taken from the second plateau. Regression equations were then determined for the anodic and cathodic transients via Equations (14) and (15), where the transient time is in s, the absolute current density is in A m^{-2}, the concentration of Na_2SO_4 is in g dm^{-3}, and the temperature is in °C. However, as the *p*-values for temperature were more than 0.05, the temperature was not statistically significant.

$$t_{anodic} = 4.55 - 4 \cdot 10^{-4} \cdot i - 0.01 \cdot c - 0.002 \cdot T \quad (14)$$

$$t_{cathodic} = 7.81 - 3 \cdot 10^{-3} \cdot i - 0.01 \cdot c + 0.016 \cdot T \quad (15)$$

Figure 13 shows the transient times modeled by Equations (14) and (15). As the temperature was not significant, the results are shown as a contour plot of the concentration of Na_2SO_4 and the current density. The concentration of Na_2SO_4 had only a minor effect. The anodic transient times were 1.6 to 2.8 s, and the effect of current density was not very strong. The cathodic transient times ranged from less than 1 s to 6.3 s, and the increase in current density had a strong effect, as it seemed to change the reaction mechanism, as shown in Figure 12.

In a typical bank of three electrode pairs operating at a constant current, the strip's cathodic current density is double that of the anodic current density. If the electrolyte is kept the same, then, with an increasing current density, the anodic and cathodic transient times will become the same. For the concentration and temperature ranges in Table 2, the anodic current densities required to achieve the same transient time were approximately 580–670 A m^{-2}. With these current densities, the transient times were 2–3 s.

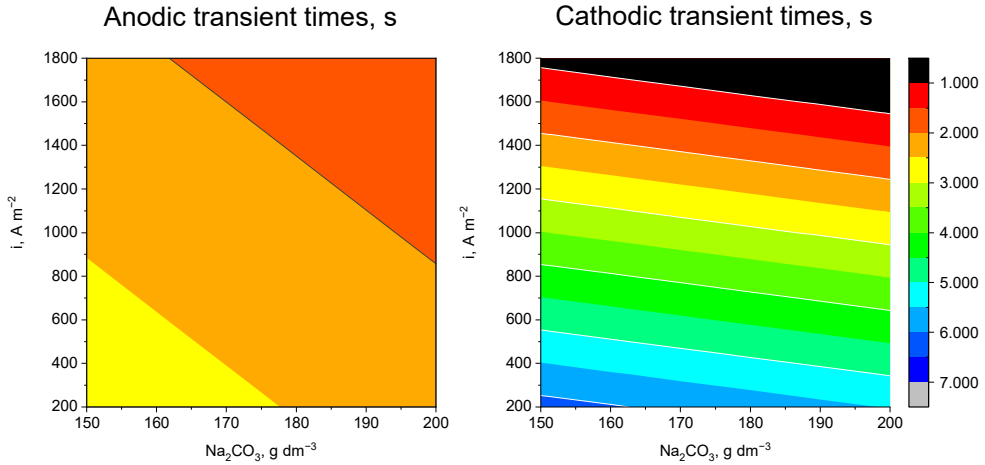

Figure 13. Modeled anodic and cathodic transient times to reach a steady potential.

The effects of the strip's velocity can be estimated by assuming the stainless steel surface to be a Randles-type equivalent circuit with a charge transfer resistance and double-layered capacitance in parallel and a solution resistance in series with this time constant. The potential of this equivalent circuit as a function of time can be calculated from Equation (16), where $V(t)$ is the potential (in V), R_Ω is the solution resistance (in Ω), R_{ct} is the charge transfer resistance (in Ω), C_{dl} is the double-layered capacitance (in F), I is the excitation current (in A), and t is the time (in s). An active system will show a gradual increase in overpotential, reaching a steady state. With the value of maximum steady-state polarization, it is possible to determine the R_{ct} and C_{dl} using Equation (17). If the time interval of the measurement is small enough, the first potential reading can be used to calculate R_Ω, with the assumption that when $t \to 0$, the electrochemical reactions have not yet started. The determination of R_{ct} and C_{dl} using Equation (17) is not dependent on the open circuit potential of the sample, but for calculating the potential using Equation (16), the OCP is needed.

$$V(t) = V(t=0) + R_\Omega \cdot I + R_{ct} \cdot I \cdot \left[1 - e^{-t/(R_{ct} \cdot C_{dl})}\right] \quad (16)$$

$$\ln(V_{max} - V_t) = \ln(R_{ct} \cdot I) - t/(R_{ct} \cdot C_{dl}) \quad (17)$$

As shown in Figure 12, the galvanostatic transient has a two-step mechanism at low current densities. When applying 200 A m^{-2}, the analysis using Equation (17) can describe the anodic pulse but not the cathodic one. An analysis using the data at 600 A m^{-2} and above indicated that the polarization became rapid. With a polarized electrode, the apparent charge transfer resistance, calculated as the slope $\partial E/\partial I$, decreased with increasing current density. With increasing current density, the surface polarized to higher overpotentials, resulting in a higher double-layered capacitance. As shown in Equation (16), when the RC time constant determined by the resistance to polarization and the double-layer capacitance became smaller, the transient time became shorter. The values of the RC time constant decreased between 200 A m^{-2} and 600 A m^{-2}, but not at higher current densities. This indicated that increasing the strip's speed should be compensated by a higher current density, but there is a limit above which this is no longer effective.

4. Conclusions

In this study, we modeled the NEP process with COMSOL Multiphysics software to study the distribution of the potential and current density at the surface of a steel strip. The aim was to find the factors that could decrease the cell's voltage or result in a more even distribution of the current and potential, thereby improving the process's energy efficiency. The results of the modeling showed that only part of the steel strip facing the electrodes was polarized to the desired potential range. The concentration of sodium sulfate and the temperature affected the electrolyte's conductivity only slightly within the studied

range. The effect of the electrolyte's conductivity on the polarization of the steel strip was concluded to be insignificant compared with the effects of the electrode-to-strip distance and the external potential.

The published literature has suggested that the pickling of steel happens in the gas evolution region, where only a fraction of the applied current is used in the reactions that remove oxide films. The kinetics of the removal of oxide film and gas evolution should be studied further to determine the time the strip must remain within the potential field. The effect of the strip's movement was investigated, with a focus on the effective time of the steel under the necessary polarization. The transient time of the steel strip as a cathode was, in general, longer than that as an anode. To have enough time for anodic polarization, the velocity of the steel strip needs to be limited. A short polarization time can be compensated by a higher applied current, but this can result in an unnecessary high cell voltage. In this study, with EN 1.4404-grade stainless steel, the maximum rate needed to provide polarization was 0.8 m/s. Further investigations with different steel grades are required to determine the effect of the steel's composition on the pickling current density and the strip's movement speed.

Author Contributions: Conceptualization, A.T.A., T.T. and E.R.; methodology, A.T.A. and J.A.; validation, A.T.A. and J.A.; formal analysis, A.T.A. and J.A.; investigation, A.T.A.; resources, M.L., T.T. and E.R.; writing—original draft preparation, A.T.A. and J.A.; writing—review and editing, T.T., E.R., M.L. and J.A.; visualization, A.T.A. and J.A.; supervision, M.L.; project administration, M.L.; funding acquisition, M.L. All authors have read and agreed to the published version of the manuscript.

Funding: This research was conducted with the funding from the TOCANEM project financed by Business Finland (grant number 41778/31/2020).

Data Availability Statement: Data are available from the corresponding author.

Acknowledgments: The authors gratefully acknowledge the support of the School of Chemical Engineering at Aalto University as well as the RawMatters Finland Infrastructure (RAMI), funded by the Academy of Finland.

Conflicts of Interest: Author Teemu Tuovinen and Elina Riekki was employed by the company Outokumpu Stainless Oy. The remaining authors declare that the research was conducted in the absence of any commercial or financial relationships that could be construed as a potential conflict of interest. The authors declare no conflict of interest. The funders had no role in the design of the study; in the collection, analyses, or interpretation of data; in the writing of the manuscript; or in the decision to publish the results.

References

1. Li, L.-F.; Celis, J.-P. Pickling of austenitic stainless steels (a review). *Can. Metall. Q.* **2003**, *42*, 365–376. [CrossRef]
2. Cheng, X.; Jiang, Z.; Wei, D.; Zhao, J.; Monaghan, B.J.; Longbottom, R.J.; Jiang, L. Characteristics of oxide scale formed on ferritic stainless steels in simulated reheating atmosphere. *Surf. Coat. Technol.* **2014**, *258*, 257–267. [CrossRef]
3. Wilson, P.R.; Chen, Z. The effect of manganese and chromium on surface oxidation products formed during batch annealing of low carbon steel strip. *Corros. Sci.* **2007**, *49*, 1305–1320. [CrossRef]
4. Cheng, X.; Jiang, Z.; Wei, D.; Hao, L.; Zhao, J.; Jiang, L. Oxide scale characterization of ferritic stainless steel and its deformation and friction in hot rolling. *Tribol. Int.* **2015**, *84*, 61–70. [CrossRef]
5. Evans, H.E.; Donaldson, A.T.; Gilmour, T.C. Mechanisms of Breakaway Oxidation and Application to a Chromia-Forming Steel. *Oxid. Met.* **1999**, *52*, 379–402. [CrossRef]
6. Hildén, J.; Virtanen, J.; Forsén, O.; Aromaa, J. Electrolytic pickling of stainless steel studied by electrochemical polarisation and DC resistance measurements combined with surface analysis. *Electrochim. Acta* **2001**, *46*, 3859–3866. [CrossRef]
7. Covino, B.S.; Scalera, J.V.; Fabis, P.M. *Pickling of Stainless Steels—A Review*; Bureau of Mines: Avondale, KD, USA, 1984.
8. Henriet, D. *Surface Treatments for Stainless Steel State of the Art-Developments and Trends: Contract No. 7210-ZZ/604 1 July 1993 to 15 November 1995*; Final Report; Office for Official Publications of the European Communities: Luxembourg, 1996.
9. Li, L.-F.; Caenen, P.; Jiang, M.-F. Electrolytic pickling of the oxide layer on hot-rolled 304 stainless steel in sodium sulphate. *Corros. Sci.* **2008**, *50*, 2824–2830. [CrossRef]
10. McCullough, H.; Fontana, M.; Beck, F. Formation of oxides on some stainless steels at high temperatures. *Trans. Am. Soc. Met.* **1951**, *43*, 404–425.

11. Ozturk, B.; Matway, R. Oxidation of type 304 stainless steels under simulated annealing conditions. *ISIJ Int.* **1997**, *37*, 169–175. [CrossRef]
12. Yearian, H.; Randell, E.; Longo, T. The structure of oxide scales on chromium steels. *Corrosion* **1956**, *12*, 55–65. [CrossRef]
13. Fabis, P.; Heidersbach, R.; Brown, C.; Rockett, T. Oxide scale formation on iron-chromium alloys in elevated temperature air environments. *Corrosion* **1981**, *37*, 700–711. [CrossRef]
14. Liu, S.; Tang, D.; Wu, H.; Wang, L. Oxide scales characterization of micro-alloyed steel at high temperature. *J. Mater. Process. Technol.* **2013**, *213*, 1068–1075. [CrossRef]
15. Meier, G.; Coons, W.; Perkins, R. Corrosion of iron-, nickel-, and cobalt-base alloys in atmospheres containing carbon and oxygen. *Oxid. Met.* **1982**, *17*, 235–262. [CrossRef]
16. Uhlig, H.H. Effect of metal composition and structure on corrosion and oxidation. *Corrosion* **1963**, *19*, 231t–237t. [CrossRef]
17. Ogushi, T. Influences of Annealing Atmosphere upon the Oxidation and Descaling Behavior of Stainless Steels. *J. Met. Finish. Soc. Jpn.* **1986**, *37*, 631–635. [CrossRef]
18. Matsuhashi, R.; Ito, S.; Nakata, M.; Oikawa, Y.; Ohmura, K. The Anodic Dissolution Behavior of Oxide Films Formed on Annealed Stainless Steels in Acidic Sulfate Solution. *Zair. Kankyo* **1993**, *42*, 576–584. [CrossRef]
19. Hildén, J.; Virtanen, J.; Ruoppa, R. Mechanism of electrolytic pickling of stainless steels in a neutral sodium sulphate solution. *Mater. Corros.* **2000**, *51*, 728–739. [CrossRef]
20. Kiya, S.; Hayashi, Y.; Kojima, T.; Hyugaji, Y. Improvement of the descalability of annealed SUS304 steel by using the vertical type direct fired heating furnace. *Tetsu Hagané* **1995**, *81*, 1007–1012. [CrossRef]
21. Chattopadhyay, A.; Bandyopadhyay, N.; Das, A.; Panigrahi, M. Oxide scale characterization of hot rolled coils by Raman spectroscopy technique. *Scr. Mater.* **2005**, *52*, 211–215. [CrossRef]
22. Zhang, M.; Shao, G. Characterization and properties of oxide scales on hot-rolled strips. *Mater. Sci. Eng. A* **2007**, *452*, 189–193. [CrossRef]
23. Nead, J.H. Treating Chromium-Iron Alloys. U.S. Patent 1,508,567, 16 September 1924.
24. Elder, F.C. Pickling Solution. U.S. Patent 1,837,118, 15 December 1931.
25. Schermer, N.H. Pickling of Stainless Steel. U.S. Patent 1,824,932, 29 September 1931.
26. Hahn, E.A. Steel Pickling Process. U.S. Patent 2,762,728, 11 September 1956.
27. Braun, E. How to improve pickling of stainless steel strip. *Iron Steel Eng.* **1980**, *57*, 79–81.
28. Fukui, S.; Yamamoto, M. Method of Electrolytically Descaling and Pickling Steel. U.S. Patent 3,429,792, 25 February 1969.
29. Fukui, S.; Yamamoto, M.; Tao, K.; Hasegawa, S. Method of Electrolytically Descaling Steel Including Selective Recovery of Dissolved Scale Products. U.S. Patent 3,04,246, 14 February 1967.
30. Machu, F. Process for Electrolytically Pickling Stainless Steels. U.S. Patent 3,043,758, 10 July 1962.
31. Shapovalov, E.; Shlyamnev, A.; Ulyanin, E.; Nikitin, V.; Fisher, A.; Goldzon, D.; Popova, L.; Milovanov, I. Investigation of operating parameters of neutral electrochemical pickling bath. *Steel USSR* **1982**, *12*, 215–219.
32. Tuovinen, T.; Vielma, T.; Lassi, U. Laboratory-scale simulation of industrial neutral electrolytic pickling as a bipolar system—Parameters affecting indirect polarization pickling of annealed stainless steel. *Eng. Rep.* **2020**, *2*, e12245. [CrossRef]
33. Fortunati, S.; Demertzis, Y.; Trasatti, S.; Giordani, P.; Musso, A.; Mancia, F. Process for Electrolytic Pickling Using Nitric Acid-Free Solutions. U.S. Patent No. 6,565,735, 20 May 2003.
34. Shapovalov, E.; Shlyamnev, A. Identification of Contactless Bipolar Pickling Mechanism of CrNi Steels in Neutral Sodium Sulphate Solution. In Proceedings of the International Conference 21st Century Steel Industry of Russia and CIS, Moscow, Russia, 6–10 June 1994; pp. 59–60.
35. Ignat'ev, V.; Sergeeva, N.; Shluger, M. An Investigation of the Process of Removing Scale with the Anodic Polarization of Austenitic Steels. *Stal* **1987**, *3*, 84–87.
36. Dunaevskii, V.; Stepanenko, V.; Shnol, M. Rate of Removal of Scale and Subscale Layer in Electrolytic Pickling of Stainless Steels in Na_2SO_4 Solution. *Prot. Met.USSR* **1985**, *21*, 359–363.
37. Frisch, B.; Thiele, W.-R.; Scholtes, E. Neutral Salt Pickling of Scaled Steel Surfaces-Optimization and Mechanisms. *Stahl Und Eisen* **1990**, *110*, 63–70.
38. Isono, T. Density, viscosity, and electrolytic conductivity of concentrated aqueous electrolyte solutions at several temperatures. Alkaline-Earth Chlorides, $LaCI_3$, Na_2SO_4, $NaNO_3$, NaBr, KNO_3, KBr, and $Cd(NO_3)_2$. *J. Chem. Eng. Data* **1984**, *29*, 45–52. [CrossRef]
39. Ipek, N.; Cornell, A.; Vynnycky, M. A mathematical model for the electrochemical pickling of steel. *J. Electrochem. Soc.* **2007**, *154*, P108. [CrossRef]
40. Ipek, N.; Holm, B.; Pettersson, R.; Runnsjö, G.; Karlsson, M. Electrolytic pickling of duplex stainless steel. *Mater. Corros.* **2005**, *56*, 521–532. [CrossRef]